Tribology Letters, Vol. 19, No. 2, June 2005 (© 2005)
DOI: 10.1007/s11249-005-5082-7

Tribochemical reactions of steel in cutting edge material during secondary wood products cutting

B. Porankiewicz[a,*] and E. Chamot[b]

[a]*Agricultural University of Poznań, Poland*
[b]*Chamot Laboratories, Naperville, USA*

Received 28 March 2004; accepted 23 January 2005

In this paper, evidence of tribochemical reactions of a steel cutting edge during cutting of Secondary Wood Products (SWP) is reported. Applying Quantum Chemical (QC) methods, with semiempirical results verified using Density Functional Theory (DFT), it was determined that some thermal degradation products of the principle components of SWP would stabilize iron, from steel and iron from the binder in cemented carbide tool materials, in an oxidized state via octahedral hydroxy organometallic complexes. Evidence for the very complex thermal degradation processes of SWP components interaction with Fe corrosion processes is also observed in Thermal Gravimetry Analysis (TGA).

KEY WORDS: cutting edge, wear, tool materials, milling, secondary wood products, tribochemical reactions, Quantum Chemistry, Thermal Degradation

1. Introduction

Tribochemical reactions, while wood and Secondary Wood Products (SWP) are being cut, have been the subject of analysis of cemented carbide cutting tools [1]. The problem of high temperature corrosion of steel tool material, however, has been discussed in the literature [2,3]. The actual conditions during high speed discontinuous cutting, including the maximum temperature in the cutting region, are not directly observable. For this reason studies have concentrated on an assumed, basic corrosion mechanism after the fact. The proposed corrosion mechanisms for high temperature corrosion of tool material, have been working hypotheses based on indirect chemical evidence (by applying some semiquantitative techniques), rather than the results of systematic investigation of the potential mechanisms [3]. Recent work on the involvement of some products of SWP thermal degradation, in tribochemical reactions, with cobalt, a binder in steel and cemented carbide tool material, via octahedral hydroxy organometalic complexes has been confirmed [1,4]. In this paper, the application of Quantum Chemical (QC) simulations, and Thermal Gravimetry Analysis (TGA), to analyzing the tribochemical reactions between Fe binder in steel and cemented carbide cutting tool materials while milling SWP is reported. Developments in the field of QC now make it possible to predict the stable geometry of organic molecules and calculate their energies to near chemical accuracy, even for intermediates and transition states which cannot be directly observed experimentally.[1,2] Extending these methods to also model transition metal compounds is an active area of research, and their degree of accuracy varies.[3]

2. Materials and methods

Thermal decomposition reactions and decomposition temperatures of the SWP components were modeled Quantum Chemically [5,6], with an Integrated Molecular Orbital/Molecular Orbital (IMOMO)[4] method that

*To whom correspondence should be addressed.
E-mail: poranek@main.amu.edu.pl

[1]For excellent introductions to the field of QC and current capabilities, see: F. Jensen, Introduction to Computational Chemistry, John Wiley & Sons, New York (1999); D. Young, Computational Chemistry: a Practical Guide for Applying Techniques to Real World Problems, John Wiley & Sons, New York (2000).

[2]E. Chamot and B. Porankiewicz, manuscript in preparation to Polymer Degradation and Stability.

[3]Chemically accurate geometries, but only qualitative relative energies of transition metal compounds can be calculated by the semiempirical, PM3tm method, for instance. Density functional theory calculations are well developed for bulk metals and avoid the spin contamination problems Hartree–Fock methods have with transition metal compounds, but gradient corrections are required to accurately model organics, and these are still evolving

[4]F. Maseras and K. Morokuma, J. Comput. Chem. 16 (1995) 1170.

combines Semiempirical level calculations with the AM1 Hamiltonian,[5] with more accurate Density Functional Theory (DFT) calculations with the Becke-Lee-Yang-Parr (BLYP)[6] functional and Double Zeta with Valence and Polarization (DZVP) basis set.[7]

A total of 54 potential, thermal decomposition reactions for the 4 major components of SWP were simulated with representative model compounds for the components and for their decomposition products. These include 7 bond dissociation reactions and 3 electrocyclic elimination reactions for Urea-Formaldehyde Resin (UFR), 14 dissociations and 2 eliminations for Melamine-Formaldehyde Resin (MFR), 19 dissociations and 4 eliminations for Lignin (Lig), and 4 dissociations and 1 elimination for Cellulose (Cel). Molecular geometries were optimized at the Semiempirical level in the program, MOPAC,[8] to a convergence criterion of Gradient Norm (GNORM)[9] 0.01 or better, and FORCE calculations were carried out to guarantee convergence to stable geometries for the energy calculations. Geometries of related model compounds were optimized by DFT, using a "fine" numeric grid and converging to a GNORM of 0.001 in the program Dgauss,[10] or to 0.006 in the program Spartan,[11] for accuracy [5]. Prediction of thermal decomposition temperatures and principle thermal decomposition products from these calculated energies is being reported elsewhere.[2] Reactions of these principle thermal decomposition products and of fragments of the four SWP components, with iron, to form hydroxide complexes, have been modeled Quantum Chemically, at the Semiempirical level with the PM3 for Transition Metals (PM3tm),[12] AM1-d,[13] Hamiltonians,[14] and at the DFT level with the BLYP, BP91,[15] or pBP[16] gradient corrected functionals, using Double Numeric with Polarization (DNP[17] and DN*[18]) basis sets [5]. The Semiempirical methods were first used qualitatively to predict the preferred spin state for each organometallic Fe complex and to screen out highly disfavored organometallic Fe intermediates based on relative energies, and to provide initial geometries for DFT calculations. Iron complexes, that at least one of the Semiempirical methods predicted would be a lower energy intermediate for Fe oxidation, were then modeled at the DFT level to calculate more accurate energies and heats of reaction.

The TGA was applied to analyze the thermal degradation of components of SWP and their interaction with Fe.

3. Results and discussion

Tribochemical reactions of cemented carbide cutting edges while milling SWP, induced by the material being

[5]Semiempirical QC method based on Neglect of Differential Diatomic Overlap approximation as developed by Dewar; M.J.S. Dewar, E.G. Zoebisch, E.F. Healy and J.J.P. Stewart, J. Amer. Chem. Soc. 107 (1985) 3902.

[6]Gradient corrected exchange and correlation functionals developed by Becke and by Lee, Yang and Parr; A.D. Becke, Phys. Rev. A. 38 (1988) 3098; C. Lee, W. Yang, and R.G. Parr, Phys. Rev. B. 37 (1988) 785.

[7]All electron basis set developed especially for density functional Gaussian-type orbital calculations. See N. Godbout, D.R. Salahub, J. Andzelm and E. Wimmer, Can. J. Chem. 70 (1992) 560.

[8]Well known program for standard semiempirical QC calculations. See M.J.S. Dewar, J. Mol. Struct. 100 (1983) 41.

[9]Mathematical term, used routinely in QC calculations as the criteria for convergence of the geometry: the scalar of the vector of derivatives of the energy with respect to the geometric variables. Convergence to a value of 0.01 or less is typically accepted as necessary for chemical accuracy (energies accurate to less than 0.1 kcal/mol) in semiempirical calculations.

[10]Commercial code implementing the DZVP basis set for Density Functional calculations, currently available from the CAChe group at Fujitsu. See also N. Godbout, D. R. Salahub, J. Andzelm and E. Wimmer, Can. J. Chem. 70 (1992) 560.

[11]Commercial program by Wavefunction, Inc., implementing the PM3tm Semiempirical and pBP Density Functional methods.

[12]Extension by Hehre of Stewart's semiempirical parameterization, PM3, to include transition metals. J.P. Stewart, J. Comp. Chem. 10 (1989) 209; J. Yu and W. Hehre, submitted to J. Comp. Chem.; K. Borve, V. Jensen, T. Karlsen, J. Stovneng and O. Swang, J. Mol. Model. 3 (1997) 193.

[13]The CAChe group's extension of the AM1 Hamiltonian by adding d-orbitals to handle transition metals.

[14]Semiempirical MOPAC calculations (including AM1 and AM1-d) and Density Functional DGAUSS calculations (including BLYP/DZVP) were conveniently carried out with the implementations and interface in the CAChe software by the CAChe group of Fujitsu.

[15]Becke's gradient corrected exchange with Perdew's correlation functionals; J. P. Perdew, in Electronic Properties of Solids '91, Eds. P. Ziesche and H. Eschrig, Akademie Verlag, Berlin (1991).

[16]Perturbative implementation of Becke's 1988 exchange functional with Perdew's 1986 correlation functional in Wavefunction's MacSpartan Pro software. See W.J. Hehre and L. Lou, "A Guide to Density Functional Calculations in Spartan," Wavefunction, Inc., Irvine, CA (1997); A.D. Becke, Phys. Rev. A. 38(6) (1988) 3098; J.P. Perdew, Phys. Rev. B 33 (1986) 8822.

[17]Numeric basis set developed for density functional calculations, comparable in size to standard, Gaussian 6-31G basis set, but more accurate, as implemented in Accelrys' DMol program. See Density Functional Methods in Chemistry, eds. J. Labanowski and J. Andzelm, Springer-Verlag, New York (1991).

[18]Spartan's version of double numeric basis set with polarization, optimized for use with the B88 and P86 functionals; see W.J. Hehre and L. Lou, "A Guide to Density Functional Calculations in SPARTAN," Wavefunction, Inc., Irvine, CA (1997).

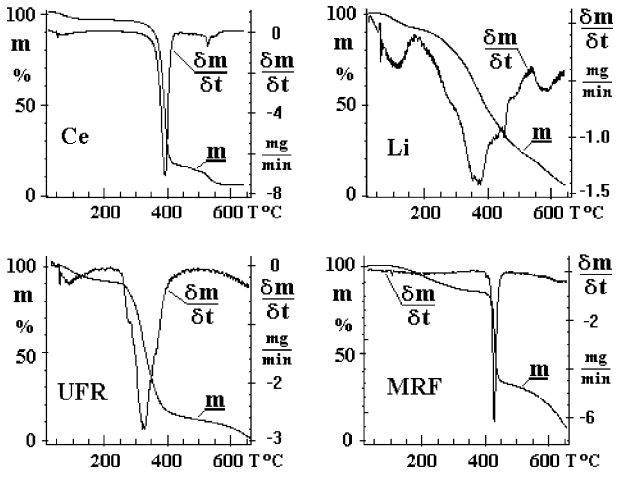

Figure 1. TGA plots, acquired for Cel, Lig, UFR and MR individually.

cut, requires chemical contact between the Fe (component of steel and addition to cemented carbide binder) and thermal decomposition products of the material being cut. Each basic component of SWP (MFR, UFR, Cel and Lig), will decompose thermally at some temperature, and the high instantaneous temperatures from heat generated by cutting friction, could lead to its thermal degradation (figure 1). Whether a specific component of SWP will decompose to generate corrosive products during milling, will depend on its decomposition temperature, and on the instantaneous cutting contact temperature, generated by increasing wear of the cutting edge [7]. The decomposition temperatures that could generate reactions observed on the TGA plots (figure 1) and from QC calculations [5] are higher in the absence of Fe in comparison to those observed in the TGA plots when Fe is present (figure 2). The presence of Fe speeds up (catalyzes) the thermal degradation of all SWP components, with cellulose the most affected. Tribochemical reactions for the Fe, probably take place much faster in comparison to the tribochemical reactions of cobalt in a cemented carbide [1,4]. The oxidation of Fe by itself, however, starts at a temperature of 160 °C (figure 3), with a maximum weight gain at a temperature of 410 °C, what would suggest larger sensitivity for high temperature corrosion. Looking at figure 4(b), however, it can be seen that there is almost no indication of corrosion interaction between Fe and products of thermal decomposition of the wood of this Indonesian wood species, there is also no weight gain up to 650 °C. These observations shows that the high temperature corrosion interaction between Fe and products of thermal degradation, during SWP cutting is very complex. The corresponding observations [8] of very high and very low High Speed Steel (HSS) cutting edge wear after milling wood specimens [8] corresponding to the TGA shown in figure 4(a) and (b) is strong evidence of high temperature corrosion interaction between iron based tool material and products of thermal degradation in some wood cases.

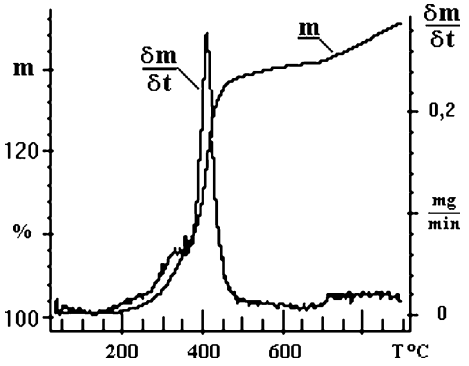

Figure 3. TGA plot, acquired for Fe alone.

Approximate electron affinities, estimated from the QC calculations for all components and decomposition products, in order to test direct electron transfer as an oxidative corrosion mechanism, are all well below the 7.9 eV first ionization potential of iron, the largest being −4.9 eV. None of the free radicals from bond homolysis, and none of the products of electrocyclic reactions, therefore, are sufficiently electron deficient to oxidize iron directly, and cause tribochemical reactions by a simple electron transfer process. In order to promote the observed oxidative corrosion of iron, specific thermal decomposition products of SWP must react chemically with the Fe during the oxidation processes, in

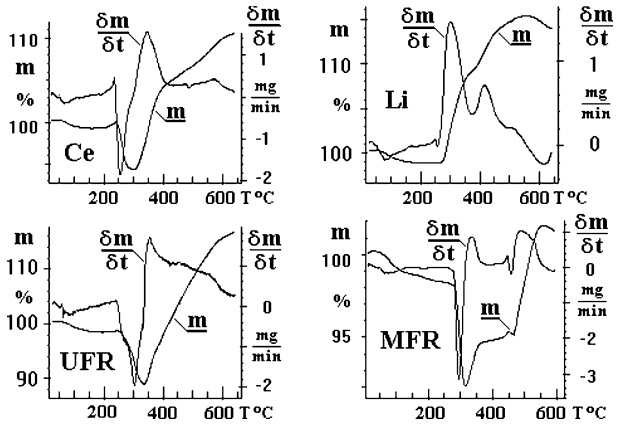

Figure 2. TGA plots, acquired for Fe mixed together with Cel, Lig, UFR and MFR.

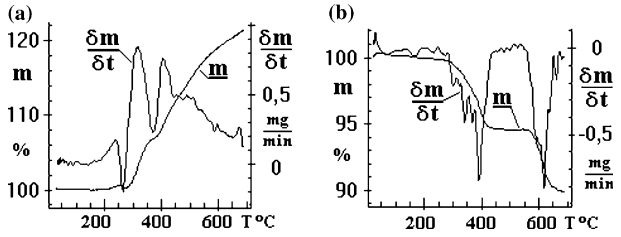

Figure 4. TGA plots, acquired for Fe mixed together with wood of two Indonesian wood species.

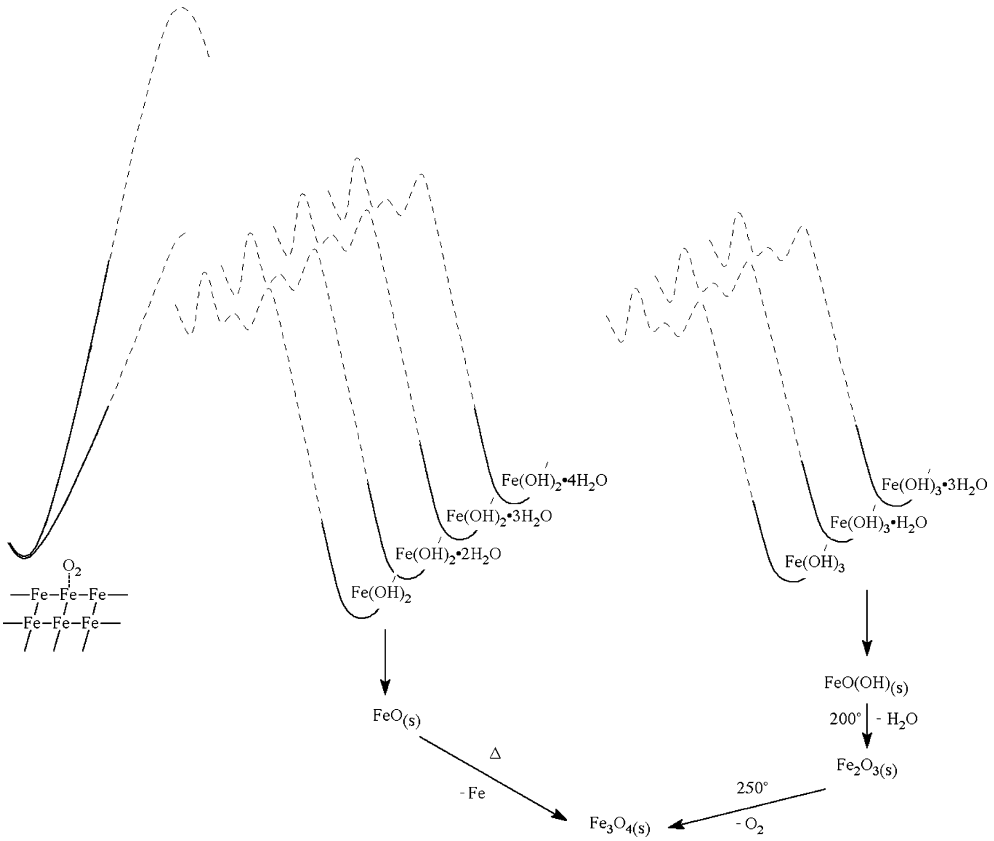

Figure 5. Reaction diagram for oxidation of Fe with and without H_2O.

some way that lowers the energy barrier to oxidation of iron. The simplest mechanism for this, would be to form an organometallic complex that stabilizes iron in an oxidized form. Specific reactions between the decomposition products and iron would also explain the relationship between tribochemical reactions and SWP components stability. Heats of reaction calculated by QC for the formation of various organometallic iron hydroxide complex intermediates, show that only certain fragments and decomposition products could stabilize iron in an oxidized form. The organometallic Fe complexes have been modeled, to consider the possibility of *HTC*-like processes during the use of steel cutting edges to cut wood. Figure 5 shows the general oxidation path for oxidation with the metal Fe. Fe hydroxide–hydrate complexes would lose water to form FeO and FeO(OH). FeO(OH) is known to condense further to form the oxide, Fe_2O_3, and when heated Fe_2O_3 is known to spontaneously release O_2 to form the mixed Fe^{+2}/Fe^{+3} oxide, Fe_3O_4. FeO is also known to spontaneously disproportionate when heated, and separate into metallic Fe and Fe_3O_4.

Iron forms octahedral complexes in both the +2 and +3 oxidation states. Fe^{+2} can also form tetrahedral complexes (to 4 ligands instead of 6), and the spin state depends on the ligands as well as the environment. The Fe oxide–hydrates are expected to be high spin (a sextet $^6A_1$, for Fe^{+3}, and a quintet $^5T_2$ for octahedral Fe^{+2} or ^5E for tetrahedral Fe^{+2}). Depending on the strength of the ligand field, some organometallic Fe complexes prefer different spin state ($^2T_2$ for Fe^{+3}, $^1A_1$ for octahedral Fe^{+2}, or $^3T_1$ for tetrahedral Fe^{+2} with strong ligand fields). All of these spin states were considered in the QC modeling. First the preferred spin state and geometry for each Fe hydroxide, as the hydrate, were determined for each QC model chemistry. Since the semiempirical methods are less well developed, they have difficulty identifying the preferred spin states correctly, so more than one method was used and the results compared. For each method, the lowest energy geometry and spin state was ultimately used as the reference energy in subsequent calculations of the effect of organometallic ligands. Tables 1 and 2 shows the calculated energies of the hydrates of $FeII(OH)_2$ and $FeIII(OH)_3$, with different methods, geometries, and spin states. Fe in the +2 oxidation state was found by both semiempirical methods, *PM3tm* and *AM1-d*, to prefer the high spin, $^5T_2$ state, in agreement with expectation. *PM3tm* also found that the trans isomer is preferred, so the energies of the high spin, trans complex were used as the *PM3tm* and *AM1-d* energies for $FeII(OH)_2 \cdot 4H_2O$ in subsequent calculations. For each QC method, the lowest energy geometry and spin state was used as the reference state.

Table 1.
Semiempirical enthalpies of iron hydroxides as octahedral hydrates.

Intermediates	Symmetry	Spin multiplicity	Semiempirical △Hf, kcal/mol	
			PM3tm	AM1-d
cis-FeII$(OH)_2 \cdot 4H_2O$	C_{2v}	1	−526.2	
		5	−582.0	
trans-FeII$(OH)_2 \cdot 4H_2O$	D_{4h}	1	−530.5	−369.3
		3		−373.9
		5	−603.3	−384.2
cis-FeIII$(OH)_3 \cdot 3H_2O$	C_{3v}	2		−396.1
		4		−390.1
		6	−565.9	−360.9
trans-FeIII$(OH)_3 \cdot 3H_2O$	C_{2v}	2	−529.5*	
		6	−578.1	

*Spin contaminated, $<s^2> = 1.78$

Density Functional calculations converged only with great difficulty, and it was not possible to calculate energies for all spin states of the hydrates. The low spin state complexes were successfully modeled with the *pBP/DN** method and the high spin states with *BLYP/DNP*. Both semiempirical *PM3tm* and Density Functional *pBP/DN** methods find the Fe^{+3} hydroxide to prefer the high spin sextet state, although they disagree on whether the cis or trans isomer is preferred for FeIII$(OH)_3 \cdot 3H_2O$. Semiempirical *AM1-d* and *SAM1* both agree with the Density Functional calculations, that the cis isomer (with the three hydroxides on the same side of the Fe, a pseudo-C_{3v} rather than a C_{2v} symmetry) is preferred, although they predict the lower spin state to be more stable. All three Density Functional methods, however, find that the most stable form is for the high spin complex to convert into a tetrahedral complex with two H_2O molecules *H*-bonded to the *OH*'s rather than coordinated to the Fe.

The potential oxidation of Fe by way of an organometallic complex intermediate with a cellulose decomposition product, levoglucosan, was modeled next at the semiempirical *PM3tm*, and the Density Functional *BP91/DNP*, *BLYP/DNP*, and *pBP/DN** levels. These results are summarized in tables 3 and 4. The *PM3tm* calculations indicated that the levoglucoside acts as a relatively weak crystal field ligand, so that the Fe complex prefers a high spin state.

The *pBP/DN** calculations confirmed this in the case of the Fe^{+3} complex, so the *BLYP/DNP* and *BP91/DNP* calculations were only done with the high spin state. The *PM3tm* calculation predicted that levoglucosan, as the tridentate di-anion, would stabilize Fe in both the +2 and +3 oxidation states (relative to the

Table 2.
Density functional energies of iron hydroxides as octahedral hydrates.

Iron Species	Symmetry	Spin multiplicity	Density functional $\triangle E_{scf}$, Hartree		
			pBP/DN*	BLYP/DNP	BP91/DNP
cis-FeII$(OH)_2 \cdot 4H_2O$	C_{2v}	1	−1721,58847		
trans-FeII$(OH)_2 \cdot 4H_2O$	D_{4h}	1	−1721,57187		
		5		−1721,44998	−1721,55227
cis-FeIII$(OH)_3 \cdot 3H_2O$	C_{3v}	2	−1720,99391		
		6	−1721,02882		
FeIII$(OH)_3 \cdot H_2O + 2H_2O$	T_d	6	−1721,05035	−1720,86943	−1720,96387
trans-FeIII$(OH)_3 \cdot 3H_2O$	C_{2v}	2	−1720,98183		
FeIII$(OH)_3 \cdot 2H_2O + H_2O$	D_{3h}	6	−1721,02225		

Table 3.
Semiempirical (PM3tm) enthalpies for formation of organometallic iron complex intermediates with levoglucosan.

Reactants		Products		Spin state	Lowest $\triangle H_{rxn}$ kcal/mol
Energies, $\triangle H_f$	kcal/mol	Energies, ΔH_f	kcal/mol		
FeII$(OH)_2 \cdot 4H_2O$ + Levoglucosan ——> FeIILevoglucoside $\cdot 3H_2O$ +			$3H_2O$		
−603.28	−208.23	−623,84	−53.43	$^1A_1$	
		−687,85		$^5T_2$	−36.6
FeII$(OH)_2 \cdot 4H_2O$ + Levoglucosan —> FeII$(OH)_2$Levoglucosan $\cdot H_2O$ +			$3H_2O$		
−603.28	−208.23	−592.03	−53.43	$^1A_1$	
		−655.74		$^5T_2$	−4.5
FeIII$(OH)_3 \cdot 3H_2O$ + Levoglucosan —> FeIII(OH)Levoglucoside $\cdot 2H_2O$ + $3H_2O$					
−578.09	−208.23	−664.04	−53.43	$^2T_2$	
		−666.08		$^6A_1$	−40.0
FeIII$(OH)_3 \cdot 3H_2O$ + Levoglucosan —> FeIII$(OH)_3$Levoglucosan +			$3H_2O$		
−578.09	−208.23	−629.85	−53.43	$^2T_2$	
		−631.40		$^6A_1$	−5.4

Table 4.
Density functional energies for formation of organometallic iron complex intermediates with levoglucosan.

Method	Reactants		Products		Spin state	Lowest $\triangle E_{rxn}$ kcal/mol
	Energies, E_{scf}, Hartree		Energies, E_{scf},	Hartree		
	$FeII(OH)_2 \cdot 4H_2O$ + Levoglucosan		—> FeIILevoglucoside $\cdot 3H_2O + 3H_2O$			
BLYP/DNP	−1721.44998	−610.82671	−2102.93370	−76.45202	$^5T_2$	−8.2
	$FeIII(OH)_3 \cdot 3H_2O$ + Levoglucosan		—> FeIII(OH)Levoglucoside $\cdot 2H_2O + 3H_2O$			
BP91/DNP	−1720.96387	−610.93353	−2102.50773	−76.46038	$^6A_1$	5.3
pBP/DN*	−1721.05035	−610.96822	−2102.57985	−76.45841	$^2T_2$	
			−2102.59453		$^4T_1$	
			−2102.61724		$^6A_1$	16.4

uncomplexed Fe hydroxide) by 36.6 and 40.0 kcal/mol respectively. But when these energies were checked with more accurate *DFT* calculations, both *BP91/DNP* and *pBP/DN*** calculations found that this complex would not stabilize the Fe^{+3} intermediate. *BLYP/DNP* calculations on the Fe^{+2} complex, however, confirmed that the cellulose fragment could stabilize the +2 oxidation state of Fe, although only by about 8.2 kcal/mol. The *PM3tm* structure of this intermediate is shown in figure 6. These results do predict that at least one of the

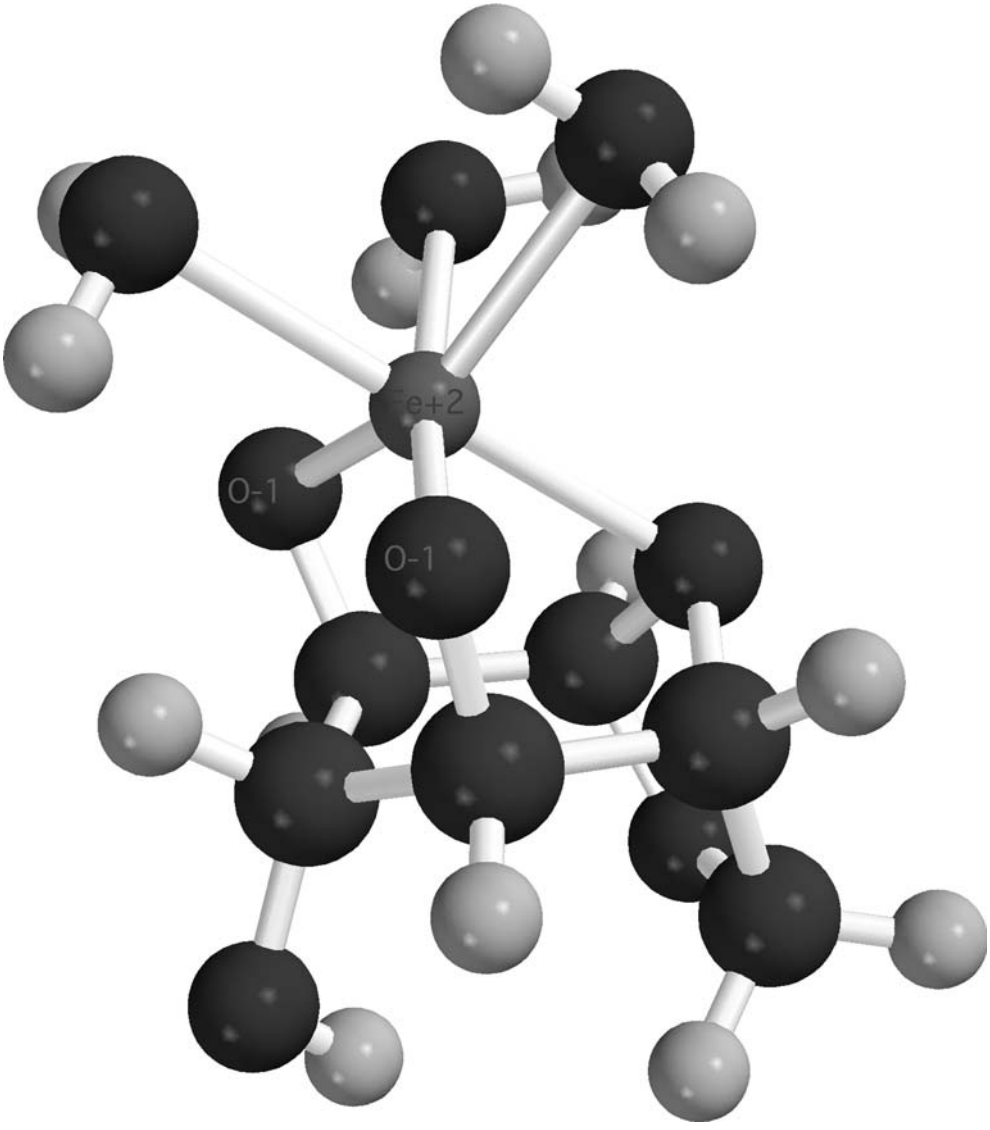

Figure 6. FeIILevoglucoside●$3H_2O$ - Organometallic Complex of Levoglucose Di-anion with Fe^{+2}.

Table 5.
Semiempirical enthalpies for formation of organometallic iron complex intermediates from MFR decomposition products.

Method	Reactants		Products		Spin State	Lowest $\cdot H_{rxn}$ kcal/mol
	Energies, ΔH_f, kcal/mol		Energies, ΔH_f, kcal/mol			
	$FeII(OH)_2 \cdot 4H_2O$ + Melamine —>		$FeII(OH)_2Melamine \cdot H_2O + 3H_2O$			
PM3tm	−603.28	28.52	−352.09	−53.43	$^1A_1$	62.4
	$FeIII(OH)_3 \cdot 3H_2O$ + Melamine —>		$FeIII(OH)_3Melamine + 3H_2O$			
PM3tm	−578.09	28.52	−339.95	−53.43	$^2T_2{}^*$	
			−356.46		$^6A_1$	32.8
	$FeIII(OH)_3 \cdot 3H_2O$ + MFRimine —>		$FeIII(OH)_3MFRimine \cdot H_2O + 2H_2O$			
PM3tm		52.32	−426.62	−53.43	$^2T_2$	−7.7
			−415.14		$^6A_1$	
AM1-d	−396.08	96.3	−153.652	−50.81	$^2T_2$	44.5
			−143.926		$^4T_1$	
			−114.254		$^6A_1$	

*Spin contaminated, $<s^2> = 0.95$

thermal decomposition products of wood itself, levoglucosan, could promote *HTC*-like corrosion of Fe from steel cutting tools. Organometallic complex intermediates from *MFR* decomposition were considered next. The results are summarized in table 5. Melamine appears to act as a weak field ligand when coordinated to the π system (high spin favored). Both *PM3tm* and *AM1-d* predict that the *MFRimine* fragment will prefer to act as a strong field ligand when coordinated to the lone pairs on nitrogen, although they disagree on whether this would stabilize the complexed intermediate. In the case of *Co*, *PM3tm* calculations had predicted that both melamine, and an *MFRimine* fragment could stabilize *Co* in the +3 oxidation state, but in the case of Fe, only the Fe^{+3} complex with *MFRimine* shows any potential stabilization. *PM3tm* calculations predict this complex to be 7.7 kcal/mol lower in energy than the uncomplexed Fe^{+3} hydroxide–hydrate, but an alternative *AM1-d* calculation contradicted this, and predicted that the *MFRimine* would also destabilize the Fe^{+3} intermediate. The *AM1-d* geometry is shown in figure 7. It is, of course, possible that some other *MFR* decom-

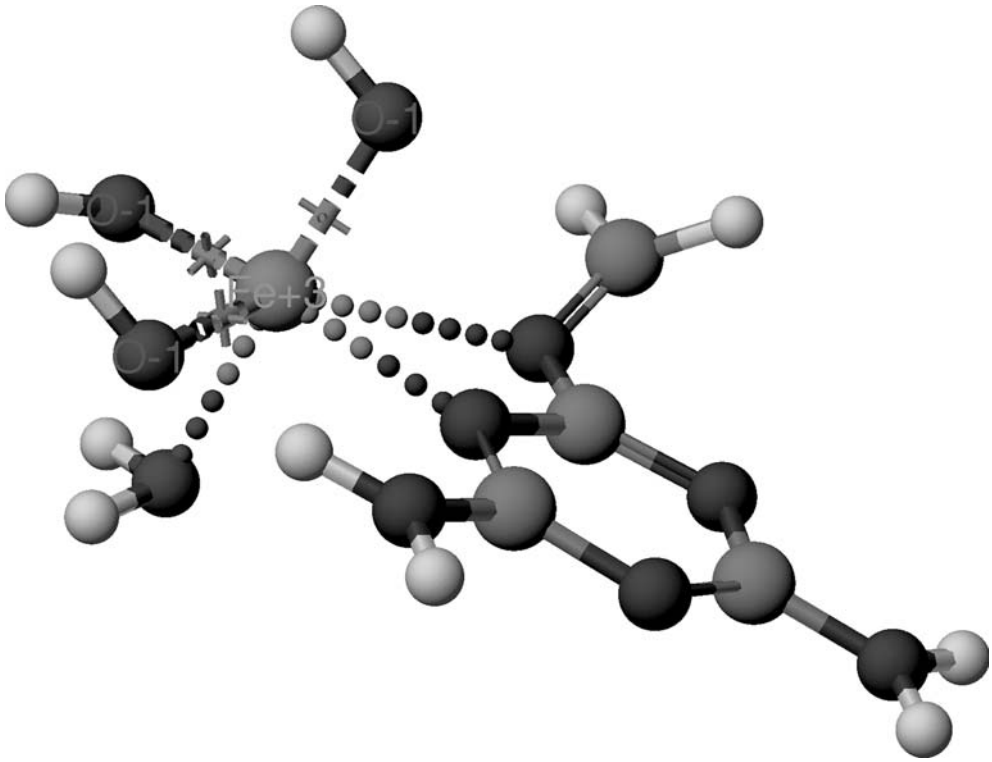

Figure 7. $FeIII(OH)_2MFRimine\bullet OH$ - Organometallic Complex of MFRimine with Fe^{+3} Hydroxide.

Table 6.
Semiempirical enthalpies for formation of organometallic iron complex intermediates from UFR.

Method	Reactants		Products		Symmetry/State	Lowest · H_{rxn} kcal/mol
	Energies, H_f, kcal/mol		Energies, H_f, kcal/mol			
$FeII(OH)_2 \cdot 4H_2O$ + UFR3mer —> $FeII(OH)_2UFR3mer \cdot H_2O + 3H_2O$						
PM3tm	−603.28	−106.54	−588.420	−53.43	$^1A_1$	−38.9
AM1-d	−384.24	−80.33	−201.347	−50.81	$^1A_1$	110.8
			−184,396		$^3T_1$	
			−186.922		$^5T_1$	
$FeIII(OH)_3 \cdot 3H_2O$ + UFR3mer —> $FeIII(OH)_3UFR3mer + 3H_2O–C_3$						
PM3tm	−578.09	−106.54	−575.30	−53.43	$^2T_2$	−51.0
			−485.39		$^6A_1$	
$FeIII(OH)_3 \cdot 3H_2O$ + UFR3mer —> $FeIII(OH)_3UFR3mer + 3H_2O–C_s$						
PM3tm	−578.09	−106.54	−573.23	−53.43	$^2T_2$	
			−594.04		$^6A_1$	−69.7
AM1-d	−396.08	−80.33	−243.165	−50.81	$^2T_2$	80.8
$FeIII(OH)_3 \cdot 3H_2O$ + UFR3mer —> $FeIII(OH)_3$ + UFR3mer + $3H_2O–C_{3h}$						
AM1-d	−396.08	−80.33	−204.379	−50.81	$^6A_1$	

Table 7.
Density functional (BLYP/DNP) energies for formation of organometallic iron complex intermediate from UFR.

Reactants		Products		Symmetry/State	Lowest ·H_{rxn} kcal/mol
Energies, E_{scf}, Hartree		Energies, E_{scf}, Hartree			
$FeIII(OH)_3 \cdot 3H_2O$ +	UFR3mer —>	$FeIII(OH)_3$ + UFR3mer +	$3H_2O–C_{3h}$		
−1720.86943	−790.24124	−2281.72033	−76.45202	$^6A_1$	21.5

position product may still be able to promote oxidation of Fe, but the specific intermediates screened here do not show evidence of being able to promote oxidation.

Finally, the involvement of organometallic complex intermediates from *UFR* decomposition was considered. This is a complicated system, and different geometries were found to be preferred, when the metal can be in different spin states. These results are summarized in tables 6 and 7. *PM3tm*, *AM1-d*, and *SAM1* semiempirical calculations all found the low spin state preferred, when the *UFR* fragment is coordinated to Fe as the symmetric, C_3 complex (with Fe coordinated symmetrically to the three ring nitrogen atoms, and the amide *H*'s forming *H*-bonds to the three hydroxyl *O*'s), but other geometries can be more stable. *PM3tm* predicts a less symmetric, C_s complex (with one *H*-bond from a hydroxyl *H* to an amide *O*) to act more like a weak field ligand, and favor a high spin complex. *AM1-d* and *SAM1* calculations both show that the high spin state would tend to dissociate to a free $Fe(OH)_3$ and an H-bonded *UFR* fragment.

The *PM3tm* calculation predicted an organometallic complex with a *UFR3mer* would lower the intermediate energy, and stabilize Fe in both the +2 and +3 states. Both *AM1-d* and *SAM1* semiempirical calculations, however, contradict this and predict these intermediates would be higher in energy. So the results were checked with Density Functional calculations. *BLYP/DNP* calculations agreed with the finding that the organometallic complex would not be stable, and would dissociate to trigonal planar $Fe(OH)_3$ and the *UFR3mer* fragment, shown in figure 8. The *BLYP/DNP* calculations also agreed with the *AM1-d* and *SAM1* calculations, and confirmed that the organometallic complex intermediate would not be lower in energy. It is possible that *UFR* fragments could be involved in the transition state for oxidation of Fe, but only as a metastable intermediate: it dissociates directly to $Fe(OH)_3$. All of the computational results, in terms of the effect on the energy barriers for oxidation of Fe, are summarized in figure 9.[19]

4. Conclusion

Semiempirical QC methods for modeling transition metal compounds did not always agree and weren't accurate enough to predict absolute energies of the potential organometallic intermediates from oxidation of iron in this study. They were useful qualitatively, to screen several reactions and select which should be more accurately modeled with Density Functional level calculations. There were differences in the absolute energies from different DFT methods, but the energy differences between reactants and products agreed to within 10 kcal/mol between methods, and confirmed

[19]Semiempirical heats of formation, ΔHj and DFT electronic energies C bold and underlined, ΔEscj in kcol/mol.

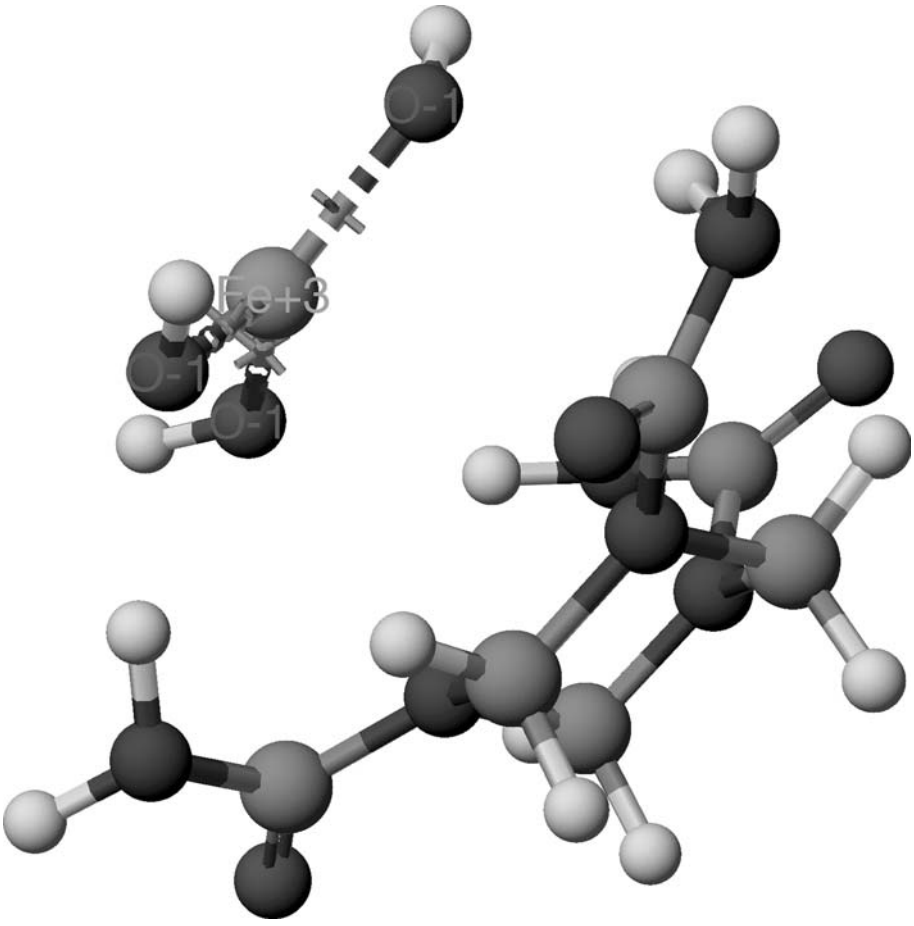

Figure 8. $Fe(OH)_3$●UFR3mer - $Fe(OH)_3$ Dissociating from Organometallic Complex with UFR3mer.

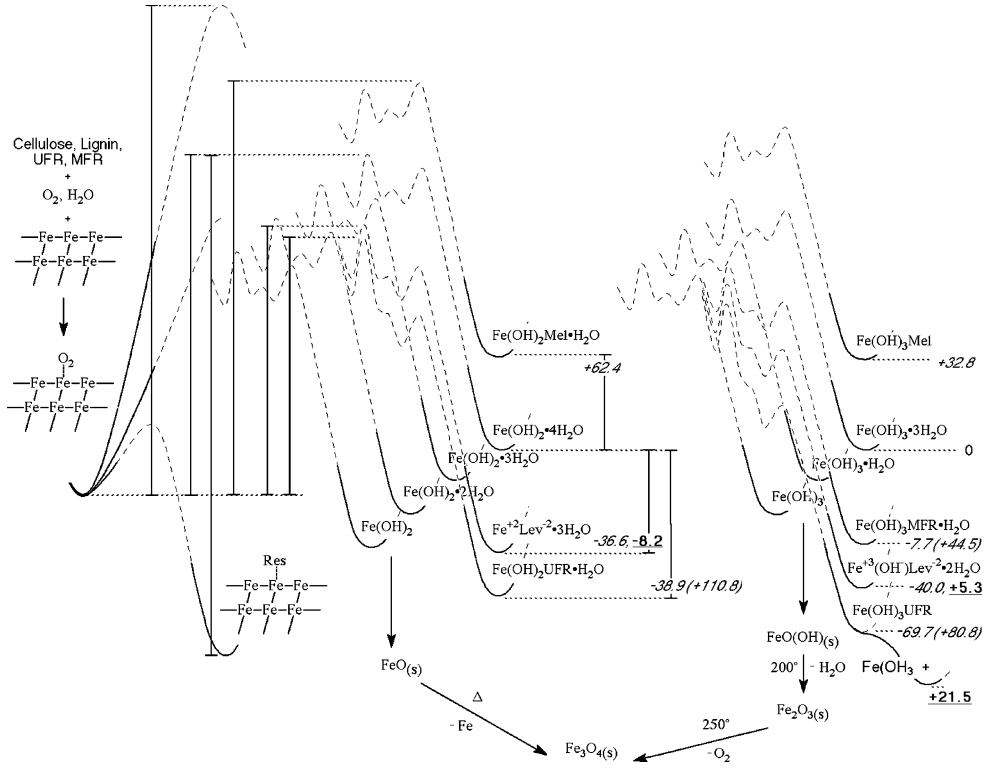

Figure 9. Effect of organometallic complex intermediates on reaction diagram for oxidation of iron.

that at least one SWP thermal decomposition product could contribute to oxidation of Fe via formation of an organometallic complex intermediate.

Specific decomposition products, which could be generated, at a maximum instantaneous temperature, may causes tribochemical reactions of iron. These reactions create organometallic complexes, which can stabilize iron in an oxidized state. Their remains can be observed after cooling down. Iron loses its binder role in the process, weakening the cutting edge material. Iron catalyzes thermal degradation of SWP components, which probably accelerates very complex tribochemical reactions. The Fe seems to be much more sensitive for tribochemical reactions in comparison to cobalt.

Acknowledgment

The work has been done in frame of project (MR/USDA-99-322), financed by Maria Skłodowska-Curie, Polish-American II Fund, Warsaw, Poland.

References

[1] B. Porankiewicz, Tribol. Lett. 13(2)(2002) 141.
[2] A.V. Mouseev, *Iznostoikost derevorezhushchego instrumenta* (Lesnaja prom, Moskva, 1981) 111.
[3] H.A. Stewart (1989). For. Prod. J. 3 (1989) 25.
[4] B. Porankiewicz, Wood Sci. Technol. 37 (2003) 47.
[5] E. Chamot and B. Porankiewicz, *Quantum Chemical Modeling of MFR and UFR Decomposition for Potential Involvement in High Temperature Corrosion During Particle Board Machining,* Proc. 13th IWMS (Vancouver, Canada, 1997), p. 741.
[6] B. Porankiewicz (2001). The investigation of chemical wear of cutting edge while processing wood and wood based products. Proj. Rep. no. MR/USDA-99-322 23.
[7] B. Porankiewicz and S. Okumura. *Theoretical Analysis of Temperature Between Cemented Carbide Cutting Edge and Wood During High Speed Contact* (Annuals of AU Poznań, Poland, CCC (1997/1998) 11.
[8] B. Porankiewicz, J. Sandak and C. Tanaka, *High Temperature Corrosion Interactions Between Cutting Edge and Wood,* Proc. 16th IWMS (Matsue, Japan, 2003), p. 741.